Ceramics International 49 (2023) 16458–16466

Contents lists available at ScienceDirect

Ceramics International

journal homepage: www.elsevier.com/locate/ceramint

Production of p-CuO/n-ZnO:Co nanocomposite heterostructure thin films: An optoelectronic study

O. Kahveci [a], A. Akkaya [b], E. Yücel [c], R. Aydın [d], B. Şahin [c,*]

[a] Department of Physics, Faculty of Sciences, Erciyes University, Kayseri, Turkey
[b] Mucur Technical Vocational Schools, Tech. Prog. Department, Kırşehir Ahi Evran University, Kırşehir, Turkey
[c] Department of Physics, Faculty of Arts and Sciences, Hatay Mustafa Kemal University, Hatay, Turkey
[d] Department of Physics, Faculty of Sciences, Selçuk University, Konya, Turkey

ARTICLE INFO

Handling Editor: Dr P. Vincenzini

Keywords:
p-n heterostructure films
CuO
ZnO
Cobalt doping
Optical properties

ABSTRACT

The p-n junction is the principal mode of optoelectronic semiconductor material. At present, we submit a solution-based attempt at the synthesis of nanostructured p-type CuO and n-type ZnO nanocomposite (NC) heterostructure films. Bare and Cobalt (Co)-doped CuO–ZnO NC films have been produced on glass slides using the SILAR (Successive Ionic Layer Adsorption and Reaction) method. The influence of Co-doping concentration on the physical characteristics of CuO–ZnO NC heterostructure films was investigated. XRD spectrums indicated the phase and structural purity of solution-based synthesized CuO–ZnO NC samples. The surface topographical, as well as optical and electrical properties of heterostructure films were, also investigated. While the bare CuO–ZnO NC film has a ~38% transmission near 1000 nm wavelength region, the 2.0% Co-doped CuO–ZnO NC film has ~31% of optical transmission. The sheet resistance value of the grown 2.0% Co:CuO–ZnO NC sample is almost 13 times lower than that of the bare CuO–ZnO NC sample at 400 K temperature. As a consequence, our attempt ensures a novel strategy for the production and performance optimization of CuO–ZnO NC heterostructures in the implementation of optoelectronics.

1. Introduction

Metal oxide nanomaterials (MONs) in single or combined form play a momentous role in many fields of solid-state physics and chemistry due to their low cost and physical and chemical properties such as favorable band edge location, high mechanical and chemical stability, tunable band gaps, light absorption over a wide range [1–4]. Additionally, MONs exhibit outstanding surface properties, high surface area, and microstructural properties that make them charming materials for the adsorption process. Because of these unique properties, MONs have been explored by scientists for a large field of applications such as catalysis, coatings, electrochemistry, energy storage devices, and sensors [5–7].

Among the MONs, copper oxide (CuO) and zinc oxide (ZnO) have special importance as technological functional oxides due to their features including being involved in the preparation of commercially available inorganic solid and economical chemical reagents. As it is known, under normal conditions, copper has two stable natural oxides: cuprous oxide (Cu_2O) and cupric oxide (CuO). Cu_2O, which has a large carrier mobility (100 cm^2 $V^{-1}s^{-1}$), is a p-type semiconductor material with a direct band gap of about 2.0 eV [8,9]. CuO is a p-type semiconductor oxide with a narrow bandgap (1.2–2.16 eV) and good intrinsic and catalytic properties. In addition, CuO materials are very non-toxic materials that can be obtained from sustainable inexpensive processes. CuO nanostructures are widely used in various applications such as rechargeable lithium-ion batteries, solar cells, gas sensors, photodetectors, and supercapacitors, due to their high theoretical capacitance, low thermal dissipation, high carrier concentration, high solar absorbance, and good electrical properties [10–12]. ZnO is a semiconductor oxide with a large exciton binding energy (60 meV), a hexagonal wurtzite lattice structure, a band gap of 3.37 eV, and an n-type character. The important properties of ZnO are great photosensitivity, high-energy radiation stability, non-toxicity, perfect piezoelectricity, mechanical-thermal stability, susceptibility to wet chemical etching, cost-effectiveness, and superior transparency in the visible area [13,14]. These features make ZnO materials beneficial in various technological utilization, such as piezoelectric devices, transparent conductive oxides, surface acoustic resonators, ultraviolet lasers, light modulators, UV detectors, anti-reflection coatings, actuators, sensors,

* Corresponding author.
E-mail address: bsahin@mku.edu.tr (B. Şahin).

https://doi.org/10.1016/j.ceramint.2023.02.007
Received 1 November 2022; Received in revised form 26 January 2023; Accepted 1 February 2023
Available online 4 February 2023

solar panels, and UV detectors [15,16].

A nanocomposite (NC) metal oxide is a combination of two or more chemically distinct and insoluble phases. The properties and performance of the composites are far superior to their components. These NC oxides are elastic and light, also have a high corrosion resistance, impact strength, and fatigue strength. Because of these characteristics, NC materials replace conventional materials used in aerospace, automotive, and other technological areas [17–19].

Although many research groups have studied both CuO and ZnO thin films before, CuO–ZnO NC thin films have rarely been investigated. Al Mamun Sakib et al. [20] obtained CuO/ZnO composites using the mechanochemical combustion method and evaluated the photocatalytic efficiency of the composites under sunlight using methylene blue as a degradation target. Çağlar et al. [6] mixed $(CuO)_x(ZnO)_{1-x}$ composite films were synthesized on glass substrates by a sol-gel spin coating technique and reported the effect of an increased Cu percentage on the structural, optical and electrical properties of the composites. Yulizar et al. [21] produced ZnO/CuO composite by green synthesis using the aqueous fraction of Theobroma cocoa bean bark extract and investigated the band gap of the composite. To improve the structural, morphological, electrical, and optical properties of CuO–ZnO NC thin films, different researchers have tried doping and improved physical properties have been obtained using various metal ion additives such as Mg, Mn, Fe, N, Al, Dy [22–26]. Among transition metals such as Mn and Fe, cobalt (Co) is a promising metal for CuO–ZnO NC doping because of its divalent state, ionic radius, and abundant electronic states. Because of these properties, the Co-doped CuO–ZnO NC displayed notable optical and magnetic manners [27,28]. Different synthesis methods, such as solid-state, spray pyrolysis, sol-gel, hydrothermal approach, Co-precipitation, and SILAR, can be used to produce CuO–ZnO NC in desired thicknesses and shapes. One of the convenient chemical methods for the production of CuO–ZnO NC is the successive ionic layer adsorption and reaction (SILAR). In this process, thin films are acquired by immersing a substrate in separately emplaced cationic and anionic precursor solutions [29–32]. SILAR is one of the simplest procedures in terms of better variety in substrate selection, reproducibility of films, and lower processing temperature for obtaining films. This technique is budget friendly, as it does not require any vacuum environment and complex experimental equipment. We have preferred the SILAR method thanks to its inexpensive, simple and convenient for large area deposition that empowers scientists experiment unconventional combination of composite thin film materials.

As far as we know, there is no study in the literature on the growth of Co-substituted ZnO/CuO NC films on glass substrates by the SILAR technique. Therefore, in this study, ZnO/CuO NC films were produced by the SILAR technique and the effect of Co^{2+} on the morphology, crystal structure, optical, and electrical properties and optoelectronic performances of the films were examined.

2. Experimental details

CuO–ZnO NC films with and without Co-doping have been produced on glass slides using the SILAR method. To prepare the sample synthesis bath, 100 ml 0.15 M Zinc acetate dehydrate (Formula: $Zn(CH_3COO)_2.2H_2O$), and 100 ml 0.15 M Copper (II) chloride dehydrate (Formula: $CuCl_2.2H_2O$) reagents were mixed at room temperature for 60 min to the obtain a well-dissolved growth bath. The pH value of the growth bath was optimized to 10.0 ± 0.02 by adding NH_4OH and then the growth bath was heated at 85 °C. The soda lime substrates were immersed in the growth bath (for 15 s) and then in deionized water (85 °C for 15 s) to remove weakly bounded materials. This synthesis process was renewed 30 times to obtain the requested thickness of CuO–ZnO NC film. To research the influence of Co^{2+} (1.0%, and 2.0%) doping on the main physical features of CuO–ZnO NC samples, two series of films were synthesized in the same procedure. These SILAR deposition processes were schematized in Fig. 1. Finally, all the films were annealed at 250 °C for 45 min in ambient air. We preferred this temperature value because of the literature on the influence of annealing treatment for nanostructured semiconductor thin films [33].

The phase and structure of the grown films were investigated using an X-ray diffractometer (A Bruker D8 Advance, Bruker AXS Inc.). The surface morphological and topographical characteristics of the obtained samples were investigated by scanning electron microscopy (SEM; Evo Ls 10) and atomic force microscope (NT-MDT/Ntegra Solaris). The elemental mapping of the samples was determined by energy-dispersive X-ray spectroscopy (EDX). The thickness of the samples was determined using a profilometer (NanoMap 500LS 3D). The optical transmittance and absorbance spectra of the grown samples were operated by UV–Vis. Spectrophotometer (Thermo Scientific, GENESYS 10S UV–Vis.). Computer-controlled Agilent B2912A Source measure unit and N1295A test fixture were used for current-voltage measurements and the SeCLaS-IC instrument control program and SeCLaS-PC parameter calculation program were used for electrical measurement and resistivity calculation [34,35]. All measurements were performed at dark and temperature-controlled test fixture units.

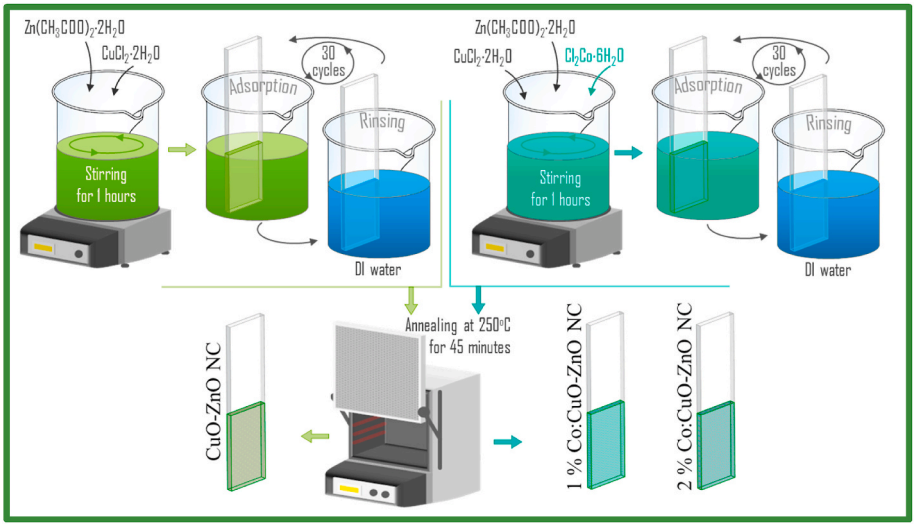

Fig. 1. Schematic representation of the SILAR deposition processes. The soda lime substrates were immersed in the growth bath (for 15 s) and then in deionized water (85 °C for 15 s) to remove weakly bounded materials. This synthesis process was renewed 30 times to obtain the requested thickness of CuO–ZnO NC film.

3. Results and discussions

To investigate the crystallographic nature of the CuO–ZnO NC thin films, X-ray diffraction technique was used. Fig. 2a shows the XRD analyses of CuO–ZnO NC thin films deposited cobalt-free, 1.0%, and 2.0% cobalt-doped. It is observed from the XRD results that all CuO–ZnO NC films fabricated by SILAR methods were deposited in a polycrystalline nature. The ZnO and CuO diffraction peaks are well matched with the JCPDS diffraction data (JCPDS 01-075-6445) and (JCPDS 00-041-0254). From these data, ZnO and CuO crystallize in hexagonal and monoclinic phases, respectively. Moreover, no characteristic diffraction peaks of other phases of copper oxide (e.g., Cu_2O) were detected in the XRD patterns of the samples. We observed from the XRD pattern of the composite films that the reflection peaks were (100), (002), (101), (102), (110), (103), (112) and (004) for the ZnO structure. Also, (002), (111), (020), (113), and (311) reflection peaks were observed for the CuO structure. The relative intensities of the ZnO (002) peaks are listed in Table 1. The intensities of the ZnO (002) peak increased with the addition of cobalt. This result showed the improved crystal quality with the addition of cobalt [36]. Compared to other samples, the highest peak intensity indicating the best crystallization was obtained in the 2.0% cobalt-doped CuO–ZnO NC thin film. It can be seen from Fig. 2b that both the diffraction line heights and ZnO (002) peak positions of 1.0%, and 2.0% cobalt-doped CuO–ZnO NC thin films are changed when compared to the undoped thin film sample. These changes in peak height and position may be due to the penetration of Co^{2+} ions into the regions in the ZnO and CuO lattice. The crystallite size (D) of the CuO–ZnO NC thin films deposited cobalt-free, 1.0%, and 2.0% cobalt-doped was estimated using the Debye-Scherrer equation [37],

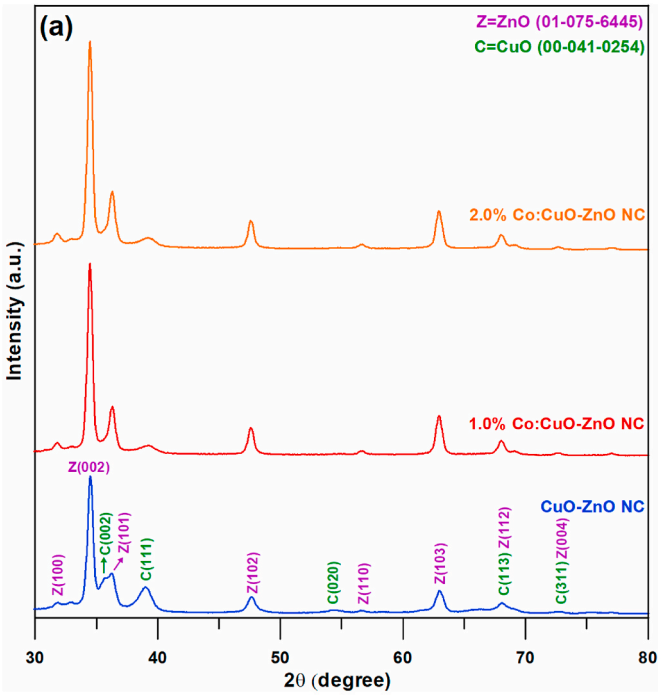

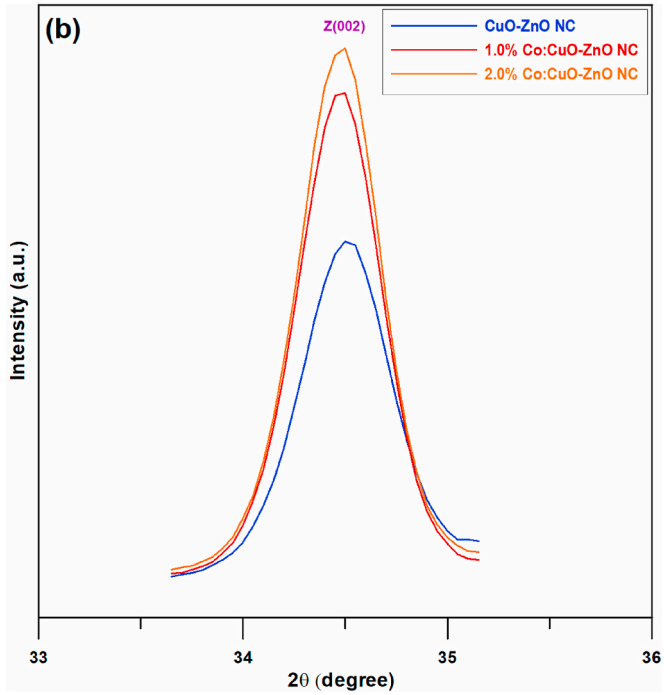

Fig. 2. **(a)** X-ray diffraction patterns of the CuO–ZnO NC films as a function of Co content in the bath solutions of the SILAR process. The ZnO and CuO diffraction peaks are well matched with the JCPDS diffraction data (JCPDS 01-075-6445) and (JCPDS 00-041-0254). From these data, ZnO and CuO crystallize in hexagonal and monoclinic phases, respectively. **(b)** ZnO (002) peak positions of CuO–ZnO NC films.

$$D = \frac{0.94\lambda}{\beta \cos\theta} \quad (1)$$

where λ is the wavelength of the incident X-ray radiation, β represents the angular width at half maximum of the peak, θ refers to Bragg's diffraction angle. Both FWHM (full-width at half maximum) values and crystallite size values of the CuO–ZnO NC samples are given in Table 1. Depending on the decrease in FWHM values, the crystallite size values of the samples increased from 17.20 to 19.03 nm. The slight increase in crystallite size caused by the addition of cobalt to the CuO–ZnO NC thin film indicates the penetration of Co^{2+} ions into the regions in the ZnO and CuO lattice. An increase in crystal size with cobalt addition has also been obtained in other studies in the literature [38–40].

There is no evidence about the direct participation of cobalt atoms in the ZnO–CuO structure was found in the XRD spectrum. But, dopant atoms cause changes in the distribution of charge centers and the magnitude of electrostatic charges in the films due to oxygen deficiency, and this is indicated by the shift in the UV–Vis spectrum. So, in native oxidation processes, all atoms are not saturated with oxygen, and the oxygen vacancy induced charge transmission (trap-assisted tunneling) model forms the basis of semiconductor behavior [41,42]. The presence of dopant atoms, such as cobalt, can cause significant changes in resistivity due to the changes in charge transfer mechanism [43,44]. ZnO is n-type semiconductors and CuO is p-type semiconductors, so, the presence of a positively charged dopant atom such as cobalt in the ZnO–CuO heterostructure can also cause a reduction of negative charge carriers [36,45]. Also, cobalt creates an additional charge centers due to oxygen deficiency as in Cu and Zn [46].

The morphological structures of CuO–ZnO NC thin films with two different concentrations (1.0% and 2.0%) Co-doped and without doping were investigated using SEM. SEM images of both doped and un-doped composite thin films at different magnifications are shown in Fig. 3. Generally, the surfaces are well-coated and have a void-free structure.

Table 1
Relative peak intensity, FWHM and crystallite size values of CuO–ZnO NC films as a function of Co content in the bath solutions of the SILAR process.

Co Concentration (%)	Relative peak intensity	FWHM (radian)	Crystallite size (nm)
	Z(002)		
0	36,600	0.00881	17.20
1.0	51,350	0.00874	17.40
2.0	55,830	0.00795	19.03

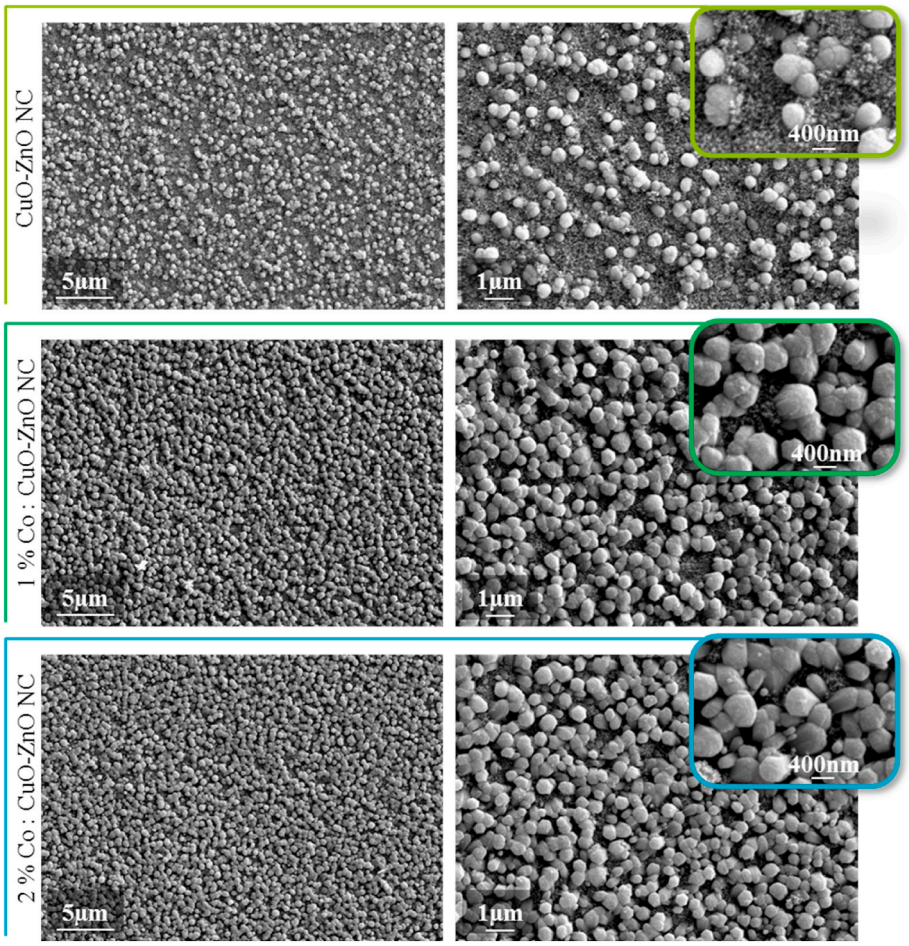

Fig. 3. SEM images of the CuO–ZnO NC films as a function of Co content in the bath solutions of the SILAR process at different magnifications. It can be seen that there are soft-edged end structures with different geometries slightly tipped on the basic structure. It can be seen that the distribution of the nanostructure tips on the surface is affected by the Co doping ratio.

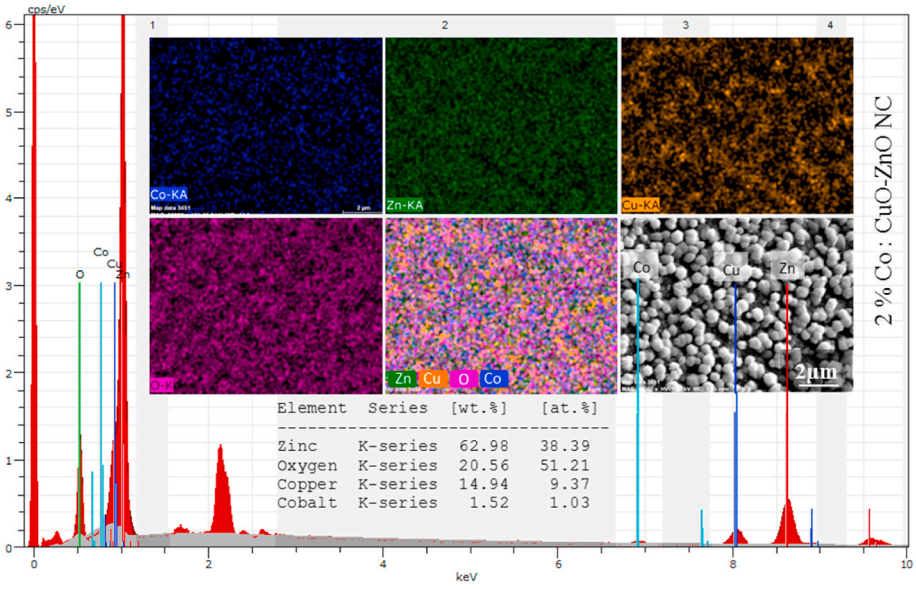

Fig. 4. EDX peak graph of the 2.0% Co:CuO–ZnO NC film, mapping images embedded in the graph and elemental analysis results. Zinc (Zn) and Oxygen (O) are the most dominant peaks, but copper (Cu) and cobalt (Co) peaks, which are the other elements in the synthesis, are also seen in the NC thin film structure.

This situation is a result observed in similar studies [47–49] and seems to be a result in harmony with the Atomic Force Microscopy (AFM) analysis in this study.

It can be seen that there are soft-edged end structures with different geometries slightly tipped on the basic structure. It can be seen that the distribution of the nanostructure tips on the surface is affected by the Co doping ratio. When the Co doping rate in the structure increases, tip-like structures are observed more intensely. Additionally, in the close images of the 2.0% Co: CuO–ZnO NC thin film with the highest doping, it is seen that the geometry of the tips becomes slightly sharper. Similarly, H. Safdar et al. [49] observed that the surface morphology of the composite films they synthesized was strongly affected by the doping concentration. The physical properties of thin films are significantly affected by their surface morphology [47]. For example, the optical bandgap values and resistivity of the NC films are different. SEM analysis of thin films becomes even more important from this perspective and for potential technological applications. The source of these structural differences can be factors such as nucleation mechanisms, synthesis methods, crystal lattice stresses, and activation energy [49–51].

The distribution of the peaks obtained from the EDX measurements, EDX-mapping, and elemental analysis results are given in Fig. 4. Zinc (Zn) and Oxygen (O) are the most dominant peaks, but copper (Cu) and cobalt (Co) peaks, which are the other elements in the synthesis, are also seen in the NC thin film structure. Elemental analysis results (weight and atomic percentage values) appear consistent with the values given in previous similar reports [36]. It also supports the presence in the structure with EDX-mapping, where the elements exhibit an almost homogeneous and uniform distribution.

AFM images of the surface topography of CuO–ZnO NC samples and their 2D and 3D topology are presented in Fig. 5. The obtained samples have a nearly homogeneous surface with tightly packed grains. The images indicate that the increasing Co content leads to a topographical

Table 2
Average roughness (Sa), root mean square (Sq), and entropy values of CuO–ZnO NC films as a function of Co content in the bath solutions of the SILAR process.

Co Concentration (%)	Average Roughness Sa (nm)	Root Mean Square Sq (nm)	Entropy
0	70.65	86.82	11.72
1.0	81.10	100.08	11.90
2.0	84.07	103.37	11.97

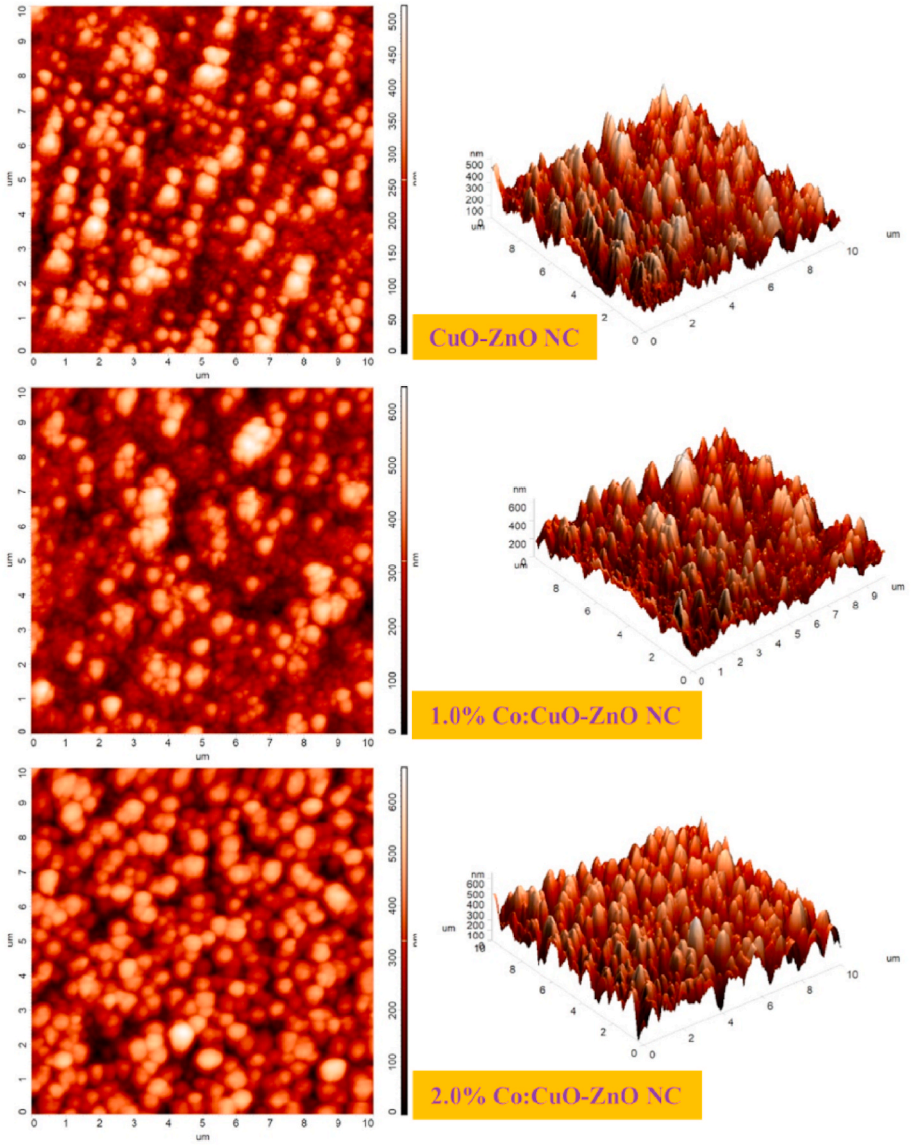

Fig. 5. 2D and 3D AFM topography images of the CuO–ZnO NC films as a function of Co content in the bath solutions of the SILAR process. The obtained samples have a nearly homogeneous surface with tightly packed grains. The images indicate that the increasing Co content leads to a topographical change.

change. The values of the root mean square (Sq) of their profile from the mean line and roughness average of a surface (Sa) were determined to quantify the surface roughness (SR) of the samples. Alteration of the film composition with metal doping influences the SR of thin film materials (Table 2). It was specified that increasing Co concentrations in the growth bath from 0 to 2.0% leads to an increase in SR of the samples (Sa from 70 nm to 84 nm, Sq from 86 nm to 103 nm, respectively).

Vibrational mode analysis of as bare CuO–ZnO and Co: CuO–ZnO NC films was performed by the FTIR method to examine the bonding configuration and the compositional analysis. FTIR spectra of bare CuO–ZnO and Co: CuO–ZnO NC films are shown in Fig. 6. Nano-structured metal-oxides in general show strong absorption peaks in the fingerprint territory (i.e. below 1000 cm^{-1}) resulting from stretching vibrations, which arise from inter-atomic vibration modes of metal-oxides. Broadened and strong peaks appearing at ~440 cm^{-1} can be assigned to the combination of Cu–O and Zn–O stretching vibration modes and absorption peaks located at 682 cm^{-1} and 875 cm^{-1} were established to the typical stretching mode of the Cu–O and Zn–O bonds [36,52,53]. The peaks, related to the stretching mode of Cu–O and Zn–O, illustrate the accomplished structure of the nanocomposite and corroborated well with the XRD results. A few vibration modes were observed in the rest of FTIR spectrum and they can be ascribed to the C═O and $–CH_2$ asymmetric and symmetric stretching vibrations from the organic contamination and residual precursors [36]. However, no significant shifts in the peaks were determined in the FTIR spectrum due to the addition of Co to CuO–ZnO NC. This confirms that there is no chemical bond exists between CuO–ZnO and Co, as seen in the XRD analysis.

The Tauc's equation was performed to estimate the optical bandgap (E_g) values for CuO–ZnO NC samples [54];

$$\alpha h\nu = C\left(h\nu - E_g\right)^{1/2} \quad (2)$$

In the equation, $h\upsilon$ is the incident photon energy and α absorption coefficient. The bandgap of CuO–ZnO NC, calculated from the optical absorbance spectra by plotting the straight line of $(\alpha h\upsilon)^2$ vs $h\upsilon$ and extrapolating the linear portion of the curve to the x-axis is presented in Fig. 7.

The estimated bandgap from the Tauc's plot is found to be 2.40 eV for bare CuO–ZnO NC and 2.29, and 2.21 eV for 1.0%, and 2.0% Co-doped CuO–ZnO NC films, respectively. Consequently, the decrease in the bandgap with the increase in Co concentration in the growth bath may be attributed to the morphological modification and structural changes confirmed in the XRD data, which might be owing to the prosperous substitution of Co^{+2} ions in the CuO and ZnO lattices. The estimated E_g values for CuO–ZnO NC samples were in good arrangement with the earlier records [47,49,55]. As defined in the alteration of XRD throughput, the Co-doping led to enlarge crystallite sizes, which further occurred in a red-shift in the optical bandgap. Additionally, the change quantity of the charge carriers in the CuO–ZnO lattice structure with Co-doping may lead to the bandgap narrowing for the produced CuO–ZnO samples, which can be ascribed to the well-known Burstein-Moss effect [56]. Thus, the E_g value of CuO–ZnO NC film has been tuned by doping it with Co to use them as a potential optoelectronic material for new technological implementation.

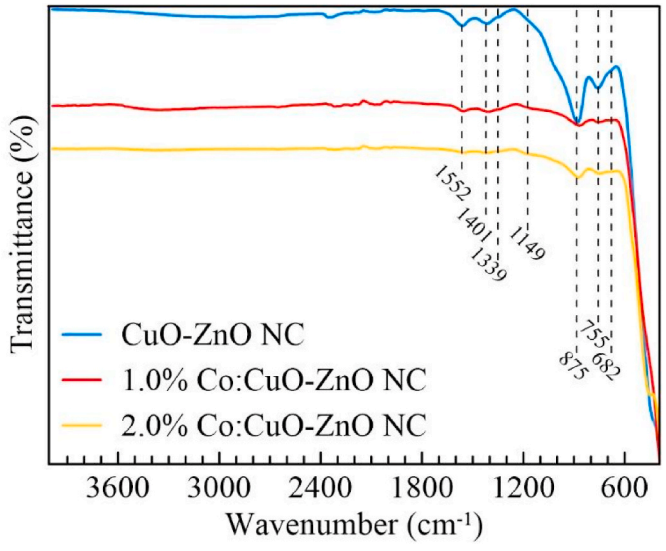

Fig. 6. FTIR spectrum of the CuO–ZnO NC films as a function of Co content in the bath solutions of the SILAR process. No significant shifts in the peaks were determined in the FTIR spectrum due to the addition of Co to CuO–ZnO NC. This confirms that there is no chemical bond exists between CuO–ZnO and Co, as seen in the XRD analysis.

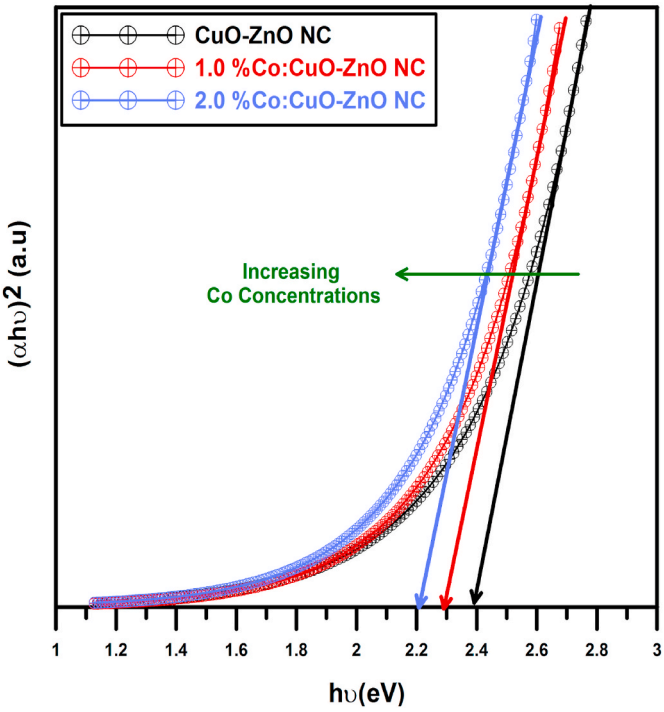

Fig. 7. Tauc plots for the determination of optical bandgap energy of the CuO–ZnO NC films as a function of Co content in the bath solutions of the SILAR process. The estimated bandgap from the Tauc's plot is found to be 2.40 eV for bare CuO–ZnO NC and 2.29, and 2.21 eV for 1.0%, and 2.0% Co-doped CuO–ZnO NC films, respectively.

Fig. 8 Exhibits the transmission spectra of CuO–ZnO NC films synthesized at two different cobalt concentrations. It can be seen that the transmission spectra of Co-doped samples are lower than the bare sample in both UV-A and visible regions. While the bare CuO–ZnO NC film has a ~38% transmission near 1000 nm wavelength region, the 2.0% Co-doped CuO–ZnO NC film has ~31% optical transmission. Generally, the alterations of transmittance depend on the factors like film thickness, surface topography and particle distribution of semiconductor materials. In this study, E_g values are determined to be diminishing regularly with raise in sample thickness. It may be owing to a change of grain boundaries, hence changing the scattering phenomena. As marked by X-ray diffractions, the crystallite size improves with an increase in Co-doping concentrations and film thickness, which changes the scattering phenomena and corresponds to the transmittance and optical bandgap [57].

Direct current (Dc) resistivity values of bare CuO–ZnO NC and Co: CuO–ZnO NC films were calculated using Ohm's Law, R = V/I, where R is the resistance, V is the applied voltage and I is the measured current at room temperature. I–V curves are linear and indicate that the ZnO/CuO

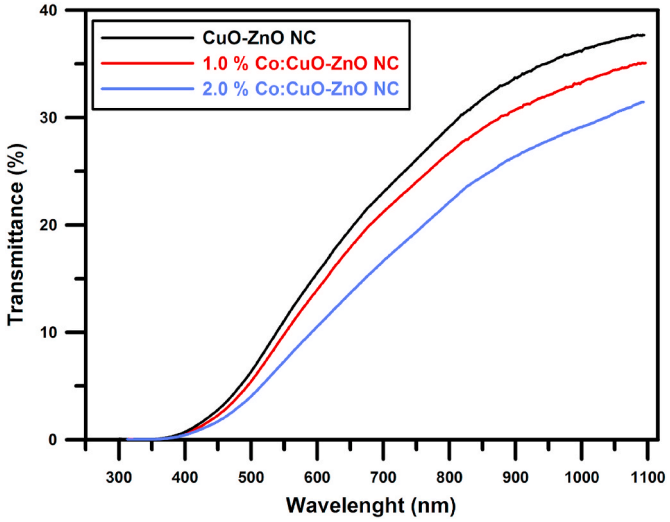

Fig. 8. Optical transmittance spectra of the CuO–ZnO NC films as a function of Co content in the bath solutions of the SILAR process. While the bare CuO–ZnO NC film has a ~38% transmission near 1000 nm wavelength region, the 2.0% Co-doped CuO–ZnO NC film has ~31% optical transmission.

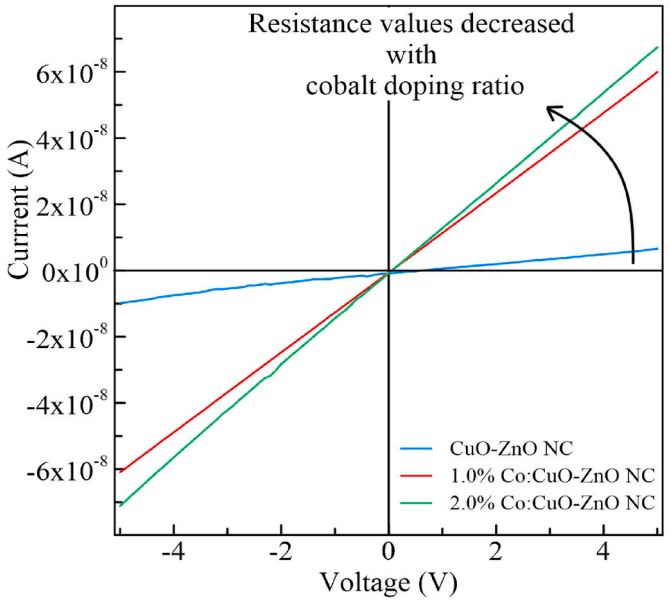

Fig. 9. I–V characteristics of the CuO–ZnO NC films as a function of Co content in the bath solutions of the SILAR process.

NC films exhibit Ohmic behavior obtained from the samples (Fig. 9). Dc resistivity values of CuO–ZnO NC film was $5.450 \times 10^8 \pm 1.452 \times 10^8\ \Omega$ and this value is close to similar reports [36,44,58,59]. Also, a definite effect of the cobalt content on the electrical transport of the CuO–ZnO NC films was observed. Dc resistivity values of 1.0% and 2.0% Co-doped CuO–ZnO NC films were $8.174 \times 10^7 \pm 1.702 \times 10^6$ and $7.075 \times 10^7 \pm 2.729 \times 10^6\ \Omega$, respectively. This decrement in dc resistivity of Co: CuO–ZnO NC films allows the successful adjustment in the electrical conductivity with doping. Also, cobalt doping has a better resistivity result than silver, aluminum, or platinum doped CuO–ZnO films [36,60,61]. These resistivity values were not used because of the nature of the thin films, which are nominally uniform in thickness. In such cases, sheet resistivity values of CuO–ZnO NC films were obtained by a well-known relation [49,62,63];

$$R_s = \rho/_t \tag{3}$$

where ρ and t are the resistivity and thickness of the deposited NC samples, respectively. Table 4 shows that the sheet resistance decreases with increasing doping ratio. This situation is usually related to the decrease in grain boundaries or scattering phenomenon of dopant electrons owing to the remarkable dopant concentrations and ionized electrons [45,49,64]. But here dopant content is very low and crystallite size and thickness is nearly constant with doping (see Tables 1 and 3). Therefore, this decrement in sheet resistance can be explained by the roles of dopant atoms in NC films. These cobalt atoms act as shallow acceptors in CuO–ZnO and cause a lower hole concentration and scattering of holes at the native defects correspond to higher mobility and lower resistance [36].

Nanostructured heterostructure film based semiconductors mostly present anomalous optical absorption and/or emission and/or conductivity owing to induced modifications in crystallinity quality, quantum confinement, electronic structure, and charge-carrier dynamics [65].

The main indicators that a material can take part in optoelectronic applications are based on many parameters such as the position of the forbidden bandgap E_g, the mobility and density of carriers, and dc resistivity [66,67]. The feasibility to tune the dc resistivity by varying the Co at % in CuO–ZnO films synthesized through the present technique would provide an opportunity for maximizing the performance of optoelectronic devices based on this and similar systems.

Fig. 10 shows the temperature dependency (in the range from 300 K up to 400 K) of the sheet resistance of bare and doped CuO–ZnO NC films and it was clear that the sheet resistance of CuO–ZnO NC samples shrinks with ascending temperature. The conductivity values rise with increasing temperature, like the general representative of semiconductor metal-oxide materials. This is the result of the ionization of shallow/defect donor-level associated electrons and ionized oxygen vacancy defects [53]. We anticipate obtained this optical bandgap and resistivity results represents an opportunity for the different technological applications.

4. Conclusion

Co:CuO–ZnO NC films were fabricated on soda-lime glass substrates using the SILAR method using a layer-by-layer deposition cycle. This research has illustrated the capability to grow composite Co:CuO–ZnO heterostructure thin films using a low-cost and environmentally friendly technique. Anymore, the comprehensive physical characteristics and the results of optical and electrical activities were discussed in detail. SEM, AFM, and XRD results exhibited that the produced thin films were nanocrystalline Co:CuO–ZnO with nanoscale-textured surfaces. The energy bandgap of bare CuO–ZnO NC was red-shifted from 2.40 to 2.21 eV as the doping weight percentage was increased to 2.0%. The detailed examinations of the conductivity properties of the sample as a function of the cobalt doping concentration displayed that a sheet resistance as low as $1.40 \times 10^9\ \Omega sq^{-1}$ was obtained with a cobalt level of 2.0%. These findings can explain p-n junction interface or optoelectronic material properties of CuO/ZnO heterostructure. Thus, the main physical characteristics of CuO–ZnO NC films have been tuned by doping them with Co to use them as potential optoelectronic material for new technological implementation.

Table 3
Film thickness and bandgap values of CuO–ZnO NC films as a function of Co content in the bath solutions of the SILAR process.

Co Concentration (%)	Film Thickness (μm)	Bandgap (eV)
0	1.17	2.40
1.0	1.28	2.29
2.0	1.33	2.21

Table 4
Sheet Resistance R_S values of CuO–ZnO NC films as a function of Co content in the bath solutions of the SILAR process.

Co Concentration (%)	Sheet Resistance (R_S) (x10^8 Ω/sq)		
	300 K	350 K	400 K
0	3.70	2.78	1.75
1.0	2.04	1.41	0.48
2.0	1.37	0.52	0.14

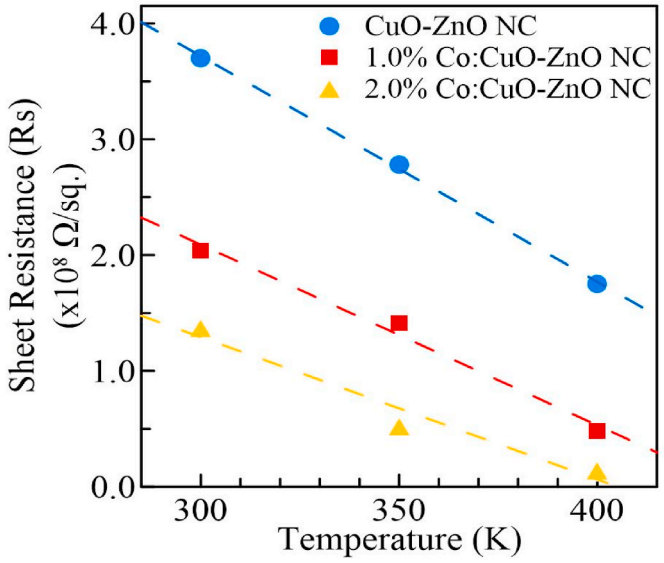

Fig. 10. The sheet resistance, as a function of temperature, for the un-doped CuO–ZnO and cobalt doped (1.0% and 2.0%) CuO–ZnO NC films. The sheet resistance value of the grown 2.0% Co:CuO–ZnO NC sample is almost 13 times lower than that of the bare CuO–ZnO NC sample at 400 K temperature.

Author contributions

O. Kahveci Data curation, Writing - review & editing, A. Akkaya Data curation, Writing - review & editing, E. Yücel Data curation, Writing-review & editing, R. Aydın Investigation, Methodology, Data curation, Writing - review & editing, B. Şahin Investigation, Methodology, Formal analysis, Data curation, Writing - review & editing, Supervision.

Data availability

The authors confirm that all data generated or analyzed during this study are included in this published article. The datasets generated and/or analyzed during the current study are available from the corresponding author on reasonable request.

Declaration of competing interest

The authors declare that they have no known competing financial interests or personal relationships that could have appeared to influence the work reported in this paper.

References

[1] R.A. Zargar, M.A. Bhat, I.R. Parrey, M. Arora, J. Kumar, A.K. Hafiz, Optical properties of ZnO/SnO_2 composite coated film, Optik 127 (2016) 6997–7001.
[2] M. Batool, R. Gill, K. Munawar, V. McKee, M. Mazhar, Single source precursor derived ZnO–PbO composite thin films for enhanced photocatalytic activity, J. Solid State Chem. 305 (2022), 122642.
[3] S.O. Aisida, A. Batool, F.M. Khan, L. Rahman, A. Mahmood, I. Ahmad, T.-k. Zhao, M. Maaza, F.I. Ezema, Calcination induced PEG-Ni-ZnO nanorod composite and its biomedical applications, Mater. Chem. Phys. 255 (2020), 123603.
[4] A. Badawi, S.S. Alharthi, M.G. Althobaiti, A.N. Alharbi, H. Assaedi, H. I. Alkhammash, N. Al-Hosiny, Structure investigation and optical bandgap tuning of La-doped CuO nanostructured films prepared by spray pyrolysis technique, Appl. Phys. A 127 (2021) 235.
[5] R. Gusain, K. Gupta, P. Joshi, O.P. Khatri, Adsorptive removal and photocatalytic degradation of organic pollutants using metal oxides and their composites: a comprehensive review, Adv. Colloid Interface Sci. 272 (2019), 102009.
[6] Y. Çağlar, D.D. Oral, M. Çağlar, S. Ilican, M.A. Thomas, K. Wu, Z. Sun, J. Cui, Synthesis and characterization of $(CuO)_x(ZnO)_{1-x}$ composite thin films with tunable optical and electrical properties, Thin Solid Films 520 (2012) 6642–6647.
[7] A.K. Srinath, L. Sankaranarayanan, R. Pandeeswari, B.G. Jeyaprakash, Thin films of α-Mn_2O_3 for resistance-based sensing of acetaldehyde vapor at ambient temperature, Microchim. Acta 182 (2015) 1619–1626.
[8] M.H. Tran, J.Y. Cho, S. Sinha, M.G. Gang, J. Heo, Cu_2O/ZnO heterojunction thin-film solar cells: the effect of electrodeposition condition and thickness of Cu_2O, Thin Solid Films 661 (2018) 132–136.
[9] S.R. Adilov, V.P. Afanaciev, I.N. Kashkul, S.E. Kumekov, N.V. Mukhin, E. I. Terukov, Studying the composition and structure of films obtained by thermal oxidation of copper, Glass Phys. Chem. 43 (2017) 272–275.
[10] N. Preda, A. Costas, M. Enculescu, I. Enculescu, Biomorphic 3D fibrous networks based on ZnO, CuO and ZnO–CuO composite nanostructures prepared from eggshell membranes, Mater. Chem. Phys. 240 (2020), 122205.
[11] S. Steinhauer, Gas sensors based on copper oxide nanomaterials: a review, Chemosensors 9 (2021) 51.
[12] Q. Zhang, K. Zhang, D. Xu, G. Yang, H. Huang, F. Nie, C. Liu, S. Yang, CuO nanostructures: synthesis, characterization, growth mechanisms, fundamental properties, and applications, Prog. Mater. Sci. 60 (2014) 208–337.
[13] R. Rajalakshmi, S. Angappane, Effect of thickness on the structural and optical properties of sputtered ZnO and ZnO:Mn thin films, J. Alloys Compd. 615 (2014) 355–362.
[14] B. Zhao, F. Mattelaer, J. Kint, A. Werbrouck, L. Henderick, M. Minjauw, J. Dendooven, C. Detavernier, Atomic layer deposition of ZnO–SnO_2 composite thin film: the influence of structure, composition and crystallinity on lithium-ion battery performance, Electrochim. Acta 320 (2019), 134604.
[15] J.E. Morales-Mendoza, F. Paraguay-Delgado, Widening UV–Vis absorption band by Cu doped ZnO and ZnO/CuO composite, Mater. Lett. 291 (2021), 129494.
[16] G.-Q. Jiang, C.-B. Yao, Z.-M. Wang, X. Wang, Y. Cai, Semiconducting ZnO&WS_2 heterojunction composite films: fabrication, characterization and ultrafast nonlinear properties, J. Alloys Compd. 863 (2021), 158664.
[17] M.H. Habibi, B. Karimi, Application of impregnation combustion method for fabrication of nanostructure CuO/ZnO composite oxide: XRD, FESEM, DRS and FTIR study, J. Ind. Eng. Chem. 20 (2014) 1566–1570.
[18] W. Fang, L. Yu, L. Xu, Preparation, characterization and photocatalytic performance of heterostructured CuO–ZnO-loaded composite nanofiber membranes, Beilstein J. Nanotechnol. 11 (2020) 631–650.
[19] C. Fan, F. Sun, X. Wang, M. Majidi, Z. Huang, P. Kumar, B. Liu, Enhanced H_2S gas sensing properties by the optimization of p-CuO/n-ZnO composite nanofibers, J. Mater. Sci. 55 (2020) 7702–7714.
[20] A.A.M. Sakib, S.M. Masum, J. Hoinkis, R. Islam, M.A.I. Molla, Synthesis of CuO/ZnO nanocomposites and their application in photodegradation of toxic textile dye, Journal of Composites Science 3 (2019) 91.
[21] Y. Yulizar, R. Bakri, D.O.B. Apriandanu, T. Hidayat, ZnO/CuO nanocomposite prepared in one-pot green synthesis using seed bark extract of Theobroma cacao, Nano-Structures & Nano-Objects 16 (2018) 300–305.
[22] M. Marzuki, N.M. Rusdi, M.Z.M. Zain, M. Izaki, Multi-staged sol–gel synthesis of Mg doped ZnO/CuO core-shell heterojunction nanocomposite: dopant induced and interface growth response, J. Sol. Gel Sci. Technol. 100 (2021) 388–403.
[23] S.M. Yakout, A.M. El-Sayed, Enhanced ferromagnetic and photocatalytic properties in Mn or Fe doped p-CuO/n-ZnO nanocomposites, Adv. Powder Technol. 30 (2019) 2841–2850.
[24] S. Rahemi Ardekani, A. Sabour Rouhaghdam, M. Nazari, N-doped ZnO-CuO nanocomposite prepared by one-step ultrasonic spray pyrolysis and its photocatalytic activity, Chem. Phys. Lett. 705 (2018) 19–22.
[25] M. Poloju, N. Jayababu, M.V. Ramana Reddy, Improved gas sensing performance of Al doped ZnO/CuO nanocomposite based ammonia gas sensor, Mater. Sci. Eng., B 227 (2018) 61–67.
[26] N.S. Kirik, B. Şahin, Characteristics modification of ZnO/CuO composite films by doping rare-earth element Dy for real-time hydration level monitoring, Micro and Nanostructures 167 (2022), 207290.
[27] A. Simimol, A.A. Anappara, H.C. Barshilia, Influence of defects on electrical properties of electrodeposited co-doped ZnO nanocoatings, Mater. Res. Express 4 (2017), 015001.
[28] A. Kaphle, T. Reed, A. Apblett, P. Hari, Doping efficiency in cobalt-doped ZnO nanostructured materials, J. Nanomater. 2019 (2019), 7034620.
[29] A. Lavín, R. Sivasamy, E. Mosquera, M.J. Morel, High proportion ZnO/CuO nanocomposites: synthesis, structural and optical properties, and their photocatalytic behavior, Surface. Interfac. 17 (2019), 100367.
[30] P. Bharathi, S. Harish, J. Archana, M. Navaneethan, S. Ponnusamy, C. Muthamizhchelvan, M. Shimomura, Y. Hayakawa, Enhanced charge transfer and separation of hierarchical CuO/ZnO composites: the synergistic effect of photocatalysis for the mineralization of organic pollutant in water, Appl. Surf. Sci. 484 (2019) 884–891.
[31] J.-H. Huang, J.-X. Chen, Y.-F. Tu, Y. Tian, D. Zhou, G. Zheng, J.-P. Sang, Q.-M. Fu, Preparation and photocatalytic activity of CuO/ZnO composite nanostructured films, Mater. Res. Express 6 (2019), 015035.

[32] B. Şahin, R. Aydın, H. Çetin, Variation of the key morphological, structural, optical and electrical properties of SILAR CdO with alkaline earth Ca^{2+} ions doping, Ceram. Int. 45 (2019) 16748–16758.
[33] B. Şahin, T. Kaya, Enhanced hydration detection properties of nanostructured CuO films by annealing, Microelectron. Eng. 164 (2016) 88–92.
[34] A. Akkaya, E. Ayyıldız, Automation software for semiconductor research laboratories: electrical parameter calculation program (SeCLaS-PC), J. Circ. Syst. Comput. 29 (2020), 2050215.
[35] A. Akkaya, E. Ayyıldız, Automation software for semiconductor research laboratories: measurement system and instrument control program (SeCLaS-IC), MAPAN 35 (2020) 343–350.
[36] A. Akkaya, B. Şahin, R. Aydın, H. Çetin, E. Ayyıldız, Solution-processed nanostructured ZnO/CuO composite films and improvement its physical properties by lustrous transition metal silver doping, J. Mater. Sci. Mater. Electron. 31 (2020) 14400–14410.
[37] G. Yıldırım, E. Yücel, Variation of the key structural, morphological, and optical properties of nanostructured copper(II) oxide (CuO) thin films using surfactant CAPB as a capping agent, J. Mater. Sci. Mater. Electron. 33 (2022) 19057–19070.
[38] M. Nirmala, A. Anukaliani, Characterization of undoped and Co doped ZnO nanoparticles synthesized by DC thermal plasma method, Phys. B Condens. Matter 406 (2011) 911–915.
[39] H.S. Al-Salman, M.J. Abdullah, Effect of Co-doping on the structure and optical properties of ZnO nanostructure prepared by RF-magnetron sputtering, Superlattice. Microst. 60 (2013) 349–357.
[40] Ş. Baturay, A. Tombak, D. Batibay, Y.S. Ocak, n-Type conductivity of CuO thin films by metal doping, Appl. Surf. Sci. 477 (2019) 91–95.
[41] L. Chabane, N. Zebbar, M.L. Zeggar, M.S. Aida, M. Kechouane, M. Trari, Effects of CuO film thickness on electrical properties of CuO/ZnO and CuO/ZnS hetero-junctions, Mater. Sci. Semicond. Process. 40 (2015) 840–847.
[42] F. Yang, M. Wei, H. Deng, Bipolar resistive switching characteristics in CuO/ZnO bilayer structure, J. Appl. Phys. 114 (2013), 134502.
[43] H. Youl Bae, G. Man Choi, Electrical and reducing gas sensing properties of ZnO and ZnO–CuO thin films fabricated by spin coating method, Sensor. Actuator. B Chem. 55 (1999) 47–54.
[44] S. Mridha, D. Basak, Investigation of a p-CuO/n-ZnO thin film heterojunction for H_2 gas-sensor applications, Semicond. Sci. Technol. 21 (2006) 928.
[45] R. Aydın, A. Akkaya, B. Şahin, Light-weight and flexible Ni-doped CuO (Ni:CuO) thin films grown using the cost-effective SILAR method for future technological requests, J. Mater. Sci. Mater. Electron. 33 (2022) 23806–23820.
[46] G.M. Joshi, M. Pai, H.R. Harrison, C.J. Sandberg, R. Aragón, J.M. Honig, Electrical properties of undoped single CoO crystals, Mater. Res. Bull. 15 (1980) 1575–1579.
[47] M. Thirumoorthi, S.S. Dhavud, V. Ganesh, T.H. Al Abdulaal, I.S. Yahia, D. Deivatamil, High responsivity n-ZnO/p-CuO heterojunction thin film synthesised by low-cost SILAR method for photodiode applications, Opt. Mater. 128 (2022), 112410.
[48] H.T. Das, S. Vinoth, M. Thirumoorthi, T. Alshahrani, H.H. Hegazy, H.H. Somaily, M. Shkir, S. Aifaify, Tuning the optical, electrical, and optoelectronic properties of CuO thin films fabricated by facile SILAR dip-coating technique for photosensing applications, J. Inorg. Organomet. Polym. Mater. 31 (2021) 2606–2614.
[49] H. Safdar, R. Aydın, B. Şahin, Syntheses, structural evolution, electrical and optoelectronic characterization of ZnO/CuO composite films doped with transition metal Mn^{2+} ions, Ceram. Int. 48 (2022) 26678–26688.
[50] E. Benrezgua, B. Deghfel, A. Zoukel, W.J. Basirun, R. Amari, A. Boukhari, M. K. Yaakob, S. Kheawhom, A.A. Mohamad, Synthesis and properties of copper doped zinc oxide thin films by sol-gel, spin coating and dipping: a characterization review, J. Mol. Struct. 1267 (2022), 133639.
[51] M.A. Khan, N. Nayan, M.K. Ahmad, S.C. Fhong, M.S. Mohamed Ali, M.K. Mustafa, M. Tahir, Interface study of hybrid CuO nanoparticles embedded ZnO nanowires heterojunction synthesized by controlled vapor deposition approach for optoelectronic devices, Opt. Mater. 117 (2021), 111132.
[52] N. Rao, M. Rao, Structural and optical investigation of ZnO nanopowders synthesized from zinc chloride and zinc nitrate, Am. J. Mater. Sci. 5 (2015) 66–68.
[53] P. Mahajan, A. Singh, S. Arya, Improved performance of solution processed organic solar cells with an additive layer of sol-gel synthesized ZnO/CuO core/shell nanoparticles, J. Alloys Compd. 814 (2020), 152292.
[54] A. Taşdemir, R. Aydın, A. Akkaya, N. Akman, Y. Altınay, H. Çetin, B. Şahin, A. Uzun, E. Ayyıldız, A green approach for the preparation of nanostructured zinc oxide: characterization and promising antibacterial behaviour, Ceram. Int. 47 (2021) 19362–19373.
[55] D. Naveena, R. Dhanabal, A. Chandra Bose, Investigating the effect of La doped CuO thin film as absorber material for solar cell application, Opt. Mater. 127 (2022), 112266.
[56] H. Güney, D. İskenderoğlu, M.E. Güldüren, K.Ç. Demir, S.M. Karadeniz, An investigation on CuO thin films grown by ultrasonic spray pyrolysis at different substrate temperatures: Structural, optical and supercapacitor electrode characterizations, Opt Mater 132 (2022), 112869.
[57] P. Matheswaran, B. Gokul, K.M. Abhirami, R. Sathyamoorthy, Thickness dependent structural and optical properties of In/Te bilayer thin films, Mater. Sci. Semicond. Process. 15 (2012) 486–491.
[58] A. Zainelabdin, G. Amin, S. Zaman, O. Nur, J. Lu, L. Hultman, M. Willander, CuO/ZnO Nanocorals synthesis via hydrothermal technique: growth mechanism and their application as Humidity Sensor, J. Mater. Chem. 22 (2012) 11583–11590.
[59] S.S. Shariffudin, N.T.C. Ibrahim, M.S.P. Sarah, H. Hashim, Effect of annealing temperature on characteristics of ZnO/CuO nanocomposite thin films, in: 2016 IEEE International Conference on Semiconductor Electronics (ICSE), 2016, pp. 177–180.
[60] B. Şahin, A. Acar, T. Kaya, Simple and low-cost synthesis of Al-doped ZnO/CuO composite nanowires for highly efficient hydration level sensing, Ceram. Int. 47 (2021) 11405–11414.
[61] M.-R. Yu, R.-J. Wu, M. Chavali, Effect of 'Pt' loading in ZnO–CuO hetero-junction material sensing carbon monoxide at room temperature, Sensor. Actuator. B Chem. 153 (2011) 321–328.
[62] K.N. Tonny, R. Rafique, A. Sharmin, M.S. Bashar, Z.H. Mahmood, Electrical, optical and structural properties of transparent conducting Al doped ZnO (AZO) deposited by sol-gel spin coating, AIP Adv. 8 (2018), 065307.
[63] D.K. Schroder, Semiconductor Material and Device Characterization, John Wiley & Sons, New York, 2006.
[64] J. Kang, G. Jo, J.-H. Ji, J.-H. Koh, Improved electrical properties of laser annealed in and Ga co-doped ZnO thin films for transparent conducting oxide applications, Ceram. Int. 45 (2019) 23934–23940.
[65] A. Sitt, I. Hadar, U. Banin, Band-gap engineering, optoelectronic properties and applications of colloidal heterostructured semiconductor nanorods, Nano Today 8 (2013) 494–513.
[66] A. Anu, M. Abdul Khadar, CuO–ZnO nanocomposite films with efficient interfacial charge transfer characteristics for optoelectronic applications, SN Appl. Sci. 1 (2019) 1057.
[67] G. Moon, W. Jang, I. Son, H.A. Cho, Y.T. Park, J.H. Lee, Fabrication of new liquid crystal device using layer-by-layer thin film process, Processes 6 (2018) 108.